



CHORUS

This is the accepted manuscript made available via CHORUS. The article has been published as:

Harnessing Mechanical Deformation to Reduce Spherical Aberration in Soft Lenses

Ahmad Zareei, Eder Medina, and Katia Bertoldi

Phys. Rev. Lett. **126**, 084301 — Published 25 February 2021

DOI: [10.1103/PhysRevLett.126.084301](https://doi.org/10.1103/PhysRevLett.126.084301)

Harnessing mechanical deformation to reduce spherical aberration in soft lenses

Ahmad Zareei[†], Eder Medina[†], and Katia Bertoldi*

School of Engineering and Applied Sciences, Harvard University, Cambridge, MA, 02148[†]

(Dated: January 25, 2021)

Mechanical deformation has recently emerged as a promising platform to realize optical devices with tunable response. While most studies to date have focused on the tuning of the focal length, here we use a combination of experiments and analyses to show that an applied tensile strain can also largely reduce spherical aberration. We first demonstrate the concept for a cylindrical elastomeric lens and then show that it is robust and valid over a range of geometries and material properties. As such, our study suggests that large mechanical deformations may provide a simple route to achieve the complex profiles required to minimize aberration and realize lenses capable of producing images of superior quality.

From programmable flexible metamaterials [1–5] and self-regulating fluidics [6, 7] to smart drug delivery systems [8–11] and scaffolds for tissue engineering [12, 13], soft materials have enabled the design of a wide range of functional structures with tunable response. In particular, inspired by the crystalline lens and ciliary muscle of the human eye, intense efforts have been devoted to the design of optical lenses with adjustable focus. To realize these tunable optical systems several strategies have been pursued. On the one hand, it has been shown that the focus can be tuned by varying the pressure of fluid enclosed by a lens-shaped flexible chamber [14–18]. On the other hand, fully solid lenses capable of focal adjustment have been realized by mechanically or electrically stretching soft membranes [19–27]. However, despite the fact that the quality of the images produced by the lenses is affected by many optical properties, including spherical aberration, tilt, coma and distortion, these design strategies predominantly consider focal point adaptation [19–27] and to a limited extent other optical properties such as astigmatism [25–27] and spherical aberration [28]. **In particular, though spherical aberration has been shown to reduce in thin lenses upon bending [28], the effect of other elastic deformations on this important optical property has not been explored yet.**

In this letter, we show that by pulling an elastomeric bi-convex lens we not only alter its focal length, but can also largely reduce its spherical aberration. While in the undeformed configuration our elastomeric lens exhibits spherical aberration - as it fails to focus all monochromatic rays to the same point (see Fig. 1a) - we find that a critical applied strain exists for which aberration is largely reduced (see Fig. 1b). We first use a combination of experiments and analysis to demonstrate the concept on a cylindrical lens and then show that the same strategy can also be extended to spherical lenses. As such, our results indicate that nonlinear deformations may provide an effective pathway to realize the complex surface profiles required for aberration-free lenses starting from simple and easy to manufacture shapes.

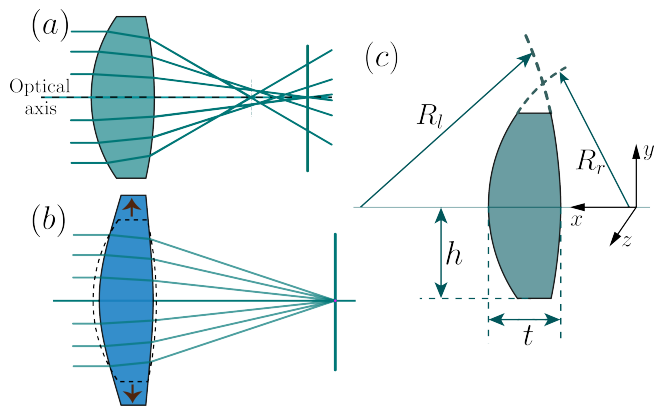


FIG. 1. Harnessing mechanical deformation to reduce spherical aberration in soft lenses. (a)-(b) Schematic of a soft lens (a) in its undeformed and (b) stretched configuration. When the lens is at rest, it exhibit spherical aberration as the rays does not converge to a single point. In the stretched configuration not only the focal length increases but also the spherical aberration may be largely reduced. (c) Schematic of the cylindrical bi-convex lens considered in this study.

We consider a cylindrical biconvex lens formed through intersection of two cylinders of radius R_r and R_l and center-to-center distance Δx that are aligned along the z -axis. Such lens has thickness $t = R_r + R_l - \Delta x$ and height $2h$, as it is truncated by two xz planes located at a distance h from the symmetry plane (see Fig. 1c). Further, it is made of an elastomeric material and is stretched by applying a y -displacement v to its top non-refracting boundary (while fixing the bottom one). We first conduct Finite Element (FE) analyses within the open-source library **Firedrake** [29] to investigate the deformation of such soft lens. We assume plain strain conditions and use higher order quadratic boundary conforming elements to mitigate mesh discretization errors of the surfaces. Moreover, we capture the material response with a compressible Neo-Hookean model with strain energy density Ψ given by

$$\Psi = \frac{\mu}{2}(\text{tr}(\mathbf{F}^T \mathbf{F}) - 3) - \mu \det(\mathbf{F}) + \frac{\mu\nu}{1 - 2\nu} \log(\det \mathbf{F})^2, \quad (1)$$

* bertoldi@seas.harvard.edu

[†] Authors contributed equally

where \mathbf{F} is the deformation gradient, μ is the shear modulus and ν is the Poisson ratio (see Supporting Information for details). For each given deformed configuration, we then use geometrical ray tracing [30] to compute the trajectories of incident rays that travel parallel to the optical axis (i.e., parallel to the x -axis). Note that, while the refractive index n generally varies with the material stress [31], for the material and range of applied deformation considered in here such changes are negligible (i.e., $\max(\Delta n) \approx 0.1\%$). As such, in our calculations we assume n to be constant.

In Fig. 2a we show the deformed configurations as well as the computed ray trajectories for a lens with $R_r/h = 1.6$, $R_l/h = 60$, $t/h = 0.72$, $\nu = 0.45$ and $n = 1.4$ at $\varepsilon = \nu/2h = 0$ (i.e., undeformed configuration) and 10.6%. Our results indicate that, while rays entering the lens near the optical axis converge at the paraxial focal point F (located at a distance f from the right surface), those that reach the lens at $y \gg 0$ intersect the optical axis at a distance $\ell(y)$ from F . For $\varepsilon = 0$, we find that $f = 3.41h$ and $\ell(y)/h \sim 0.28(y/h)^2$. Differently, for $\varepsilon = 10.6\%$ the paraxial focal point distance increases to $3.82h$ and $\ell(y) \sim 0$. As such, these results indicate that the applied deformation not only enables us to tune the focus of the lens, but can also be exploited to reduce its aberration.

In order to better quantify the effect of the applied deformation on aberration, we introduce a longitudinal measure of the spherical aberration, $\mathcal{L} = \max \ell(y)$ for $y \in [-0.8h, 0.8h]$, where this range is chosen to avoid highly nonlinear boundary effects [32]. In Fig. 2b we plot the evolution of both the paraxial focal point distance, f , and longitudinal measure of the spherical aberration, \mathcal{L} , as a function of the applied strain, ε . The results indicate that, while f increases linearly with ε , \mathcal{L} first decreases, reaches a minimum at $\varepsilon = \varepsilon_{\min} = 10.6\%$ and then further increases. To gain more insight into the physical ingredients underlying the observed phenomenon, we examine the deformed shape of the stretched lens. Towards this end, in Fig. 2c we report the maximum principal stretch, λ_{\max} , and its directions at ε_{\min} . We find that the deformation is minimal in the region close to the left surface near the optical axis, so that the initial spherical curvature is preserved there. However, away from the optical axis the lens deforms non-uniformly making the surfaces deviate from their initial spherical profile — a fact that is known to promote reduction in spherical aberration [33].

Next, to validate our numerical findings, we fabricate a lens identical to that considered in Fig. 1b (with $t = 18\text{mm}$) out of a transparent silicone elastomer (Slygard 184 - see Supporting Information for details). In our tests we clamp the lens at its flat boundaries and use a linear stage motor (ThorLabs-LTS300) to stretch it (See Fig. 2c). At different levels of applied deformation we then scan the left surface of the lens with a laser (LT-301 500mW) mounted on a separate linear stage and pointed parallel to lens optical axis, while recording the trajectories of the reflected ray with a camera (SonyRX400 - see Supporting Information for details). We find the ex-

perimental results nicely match both the deformed shape (Fig. 2d) as well as the evolution of f and \mathcal{L} (Fig. 2b) predicted by our numerical analyses, with small discrepancies due to unavoidable imperfections introduced during fabrication and testing. As such, these results confirm that pulling a biconvex lens, in addition to increasing its focal length, also reduces the longitudinal measure of spherical aberration.

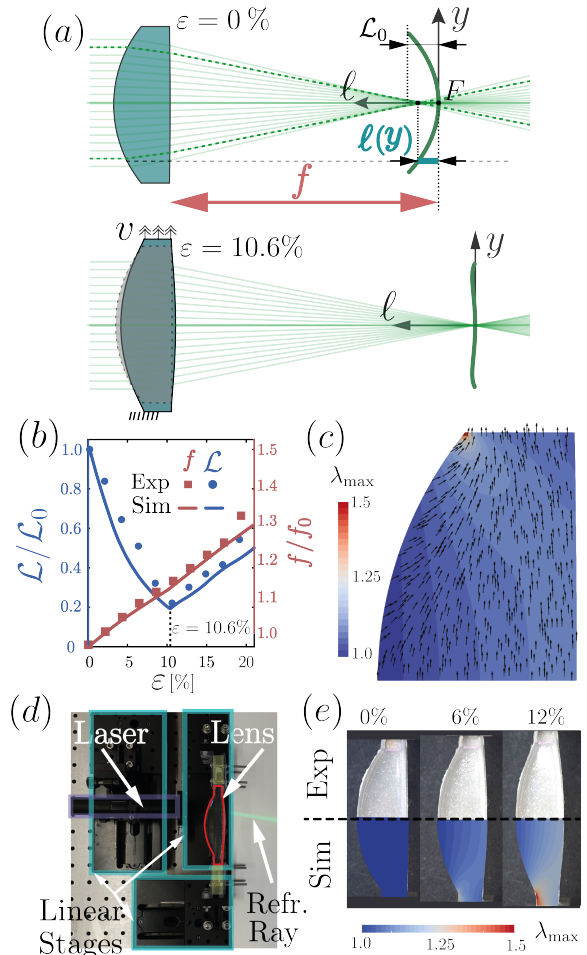


FIG. 2. Pulling of a bi-convex cylindrical lens with $R_r/h = 1.6$, $R_l/h = 60$, $t/h = 0.72$. (a) Ray trajectories at $\varepsilon = 0\%$ (top) and $\varepsilon = \varepsilon_{\min} = 10.6\%$ (bottom). (b) Evolution of $\mathcal{L}/\mathcal{L}_0$ (blue) and f/f_0 (red) as a function of ε , where $\mathcal{L}_0 = \mathcal{L}(\varepsilon = 0) = 0.05h$ and $f_0 = f(\varepsilon = 0) = 5.6h$. Both experimental (markers) and numerical (solid lines) results are shown. (c) Numerically predicted magnitude and direction of the maximum principal stretch at $\varepsilon = \varepsilon_{\min} = 10.6\%$. (d) Experimental setup. (e) Experimental (top) and numerical (bottom) snapshots of the lens at different level of applied deformation. For the numerical images, we also show the the maximum principal stretch λ_{\max} in the deformed configurations.

The deformation-induced reduction in longitudinal aberration observed in both experiments and simulations (Fig. 2b) suggests that at a critical strain the lens surface approaches the profile of a perfect zero-aberration

lens. To quantify the agreement between the two geometries, we first analytically derive the surface profile for an aberration-free lens and then compare it with that of our stretched lens. To this end, we use Fermat's principle which states that incident rays emanating from the same source plane and converging at an identical point must have equal optical path lengths. In particular, we consider the optical path of an arbitrary far-field ray that enters the left lens surface point Q , exits at the right surface at point P and intersects the optical axis at the focal point at angle an angle θ . The optical path length of such ray between the yz -plane passing through the leftmost point of the lens and the focal point is given by

$$\Lambda^P = n_0(f + L_0 - L(\theta) - x_P) + n \frac{L(\theta)}{\cos(\delta)} + n_0 \sqrt{x_p^2(\theta) + y_p^2(\theta)}, \quad (2)$$

where n_0 denotes the refractive index of the surrounding medium, $L(\theta)$ represents the horizontal distance travelled through the lens, $L_0 \equiv L(\theta = 0)$ and (x_p, y_p) are the coordinates at point P . Moreover, δ is the angle between the horizontal axis and the in-lens ray path (Fig. 3a), which is determined by Snell's law

$$n \sin(\psi + \delta) = n_0 \sin(\theta + \psi), \quad (3)$$

with $\psi = \tan^{-1}(dx_P/dy_P)$. Note that the first, second and third terms in Eq. (2) denote the optical distances travelled by the off-axis ray to (i) arrive at point Q from the selected yz -plane, (ii) traverse the lens, and (iii) reach the focal point from point P. Since for a ray travelling along the optical axis (for which $\theta = 0$ and $y_p = 0$) Eq. (2) reduces to

$$\Lambda^{ax} = nL_0 + n_0f, \quad (4)$$

the aberration-free lens at each level of applied strain is calculated by imposing $\Lambda^P = \Lambda^{ax}$, while inputting the right surface coordinates, (x_p, y_p) , focal distance, f , and deformed lens thickness, L_0 , obtained in the FE simulation [34]. In Fig. 3b we analyze the difference in the coordinates of the left surface of the aberration-free lens defined by $\mathbf{x}^{Ana} = (x_p + L(\theta)/\cos \delta, y_p + L(\theta)/\sin \delta)$ and the simulated coordinates, \mathbf{x}^{FE} , by looking at their L^2 -norm difference for $y \in (0, 0.8h)$ as a function of the applied strain ε . We find that the surface quickly approaches the aberration-free profile and then gradually deviates from it at larger strains, with the L^2 -norm difference that reaches a nonzero minimum at ε_{\min} . As such, these results indicate that the nonlinear deformation caused by applied strain ε_{\min} results in a lens profile with non-constant curvature very close to that required to remove aberration in a bi-convex cylindrical lens. To further understand the effect of the applied deformation on aberration, we plot the difference between the aberration-free and stretched profiles along the lens height. The results reported in Fig. 3c show that different regions of the lens approach the aberration free surface

at different rates. As the strain is applied the entire lens converges towards the aberration-free profile until a small difference is reached at ε_{\min} . Any additional deformation then causes the region next to the boundaries to diverge while the inner region continues to converge closer to the aberration-free profile. These two contrasting trends lead to an increase of L^2 -norm difference between the coordinates of the left surface of the aberration-free lens for $\varepsilon > \varepsilon_{\min}$. Therefore, our results indicate that the combined deformations of the right and left surface, and the change in the lens thickness caused by the applied deformation contribute in a complex way to the observed reduction in aberration.

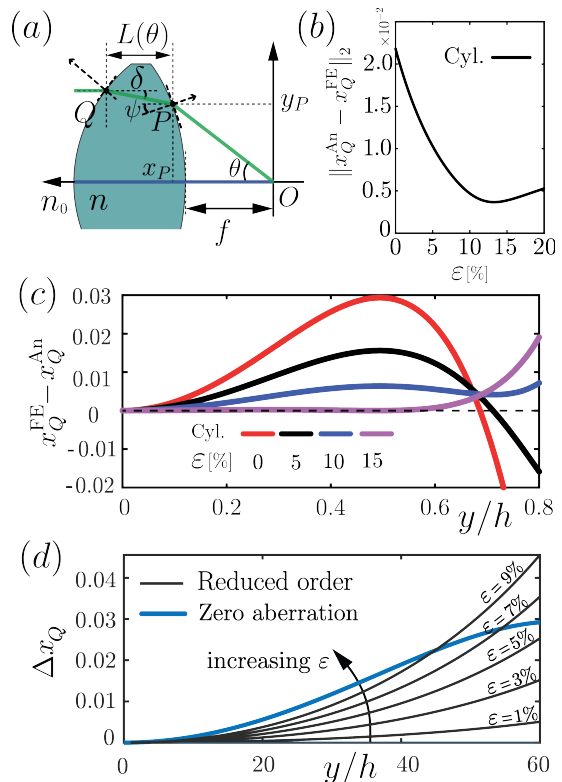


FIG. 3. Aberration-free profiles. (a) Schematic of our cylindrical biconvex lenses. (b) Evolution of L^2 -norm difference between the coordinates of the left surface of the aberration-free lens and the simulated one, $\|x_Q^{An} - x_Q^{FE}\|_2$, as a function of the applied strain, ε for the lens considered in Fig. 2. (c) Difference between the stretched profile and an aberration-free profile, $x_Q^{FE} - x_Q^{An}$, along the lens height, y/h . (d) Left surface deviation from its initial configuration at different strains predicted by the reduced order model (black lines), and the deviation required for a zero-aberration lens surface (blue line).

Next, to further elucidate the effect of deformation on aberration reduction, we developed a reduced order model where we describe the cylindrical lens as a series of infinitesimal hyperelastic rectangular elements undergoing uniaxial deformation and assume that the right surface remains flat throughout the stretching process (see Supporting Information for details). This simple model

allows us to describe the left surface profile as a function of applied strain and, therefore, quantify the effect of stretching on aberration. In Fig. 3d we plot the left surface deviation from its initial configuration at different strains predicted by the reduced order model (black lines), and the deviation required for a zero-aberration lens surface (defined by Eqs. (2)-(4) - blue line). In agreement with the results of our FE simulations, we find that the left surface of the lens approaches the profile of a zero aberration lens as ε increases, but the profiles never fully coincide. As such, the reduced order model points to the robustness of the observed phenomenon, as it shows that the stretching-induced reduction in aberration can be observed as geometric parameters are varied.

Having demonstrated that the applied deformation can be exploited to largely reduce aberration in a cylindrical lens, we now show that the phenomenon persists for a wide range of geometrical and material properties and that can be also extended to spherical lenses. In Figs. 4a-d we report the numerically predicted evolution of \mathcal{L} as a function of the applied deformation for a large set of cylindrical lenses as well as spherical ones, which are deformed by radially stretching their non-refracting boundaries (see Supporting Information for details). The results indicate that regardless of geometry and Poisson's ratio, the applied stretching can be harnessed to reduce aberration of both cylindrical and spherical biconvex lenses by $\sim 85\% - 90\%$. Further, by comparing the response of the spherical and cylindrical lenses, we find that the former require a smaller applied strain to minimize \mathcal{L} . The results of Fig. 4a-d also show that for all sets of considered parameters the aberration curves follow a similar trajectory (i.e., decreasing to a minimum reached and increasing afterward) with the strain at which the aberration is minimum, ε_{\min} , determined by a complex interplay between mechanics, geometry, and optical properties. The dependence of ε_{\min} to various geometrical parameters can be extracted from our numerical results and can be used for the lens design (see Supporting Information for details). We further like to point out that ε_{\min} not only depends on geometrical and material parameters, but also it depends on the aperture size (i.e., the area of the lens considered). A smaller aperture results in smaller initial aberration. However, since the central region of the lens is slower in approaching the zero aberration profile, ε_{\min} becomes larger (see Fig. S4). Remarkably, the aberration reduction persists independent of geometrical and material properties and initial aperture size.

While the proposed concept is robust with respect to geometric variations, it is important to recognize that the direction of the applied deformation plays a crucial role. As shown in Fig. 4e, differently from the pulling considered thus far, an applied compressive deformation further accentuates the initial aberration as it locally changes the lens' surfaces to move them away from the aberration-free profiles (see Fig. S3). Differently, a compression load may reduce aberration in a bi-concave lens (see Fig. 4f

for a lens characterized by $R_r/h = -60$, $R_l/h = -1.6$ and $t/h = 0.32$), but such reduction is limited to small levels of strain as under compression a buckling instability is triggered that significantly alters its geometry (Movie S1).

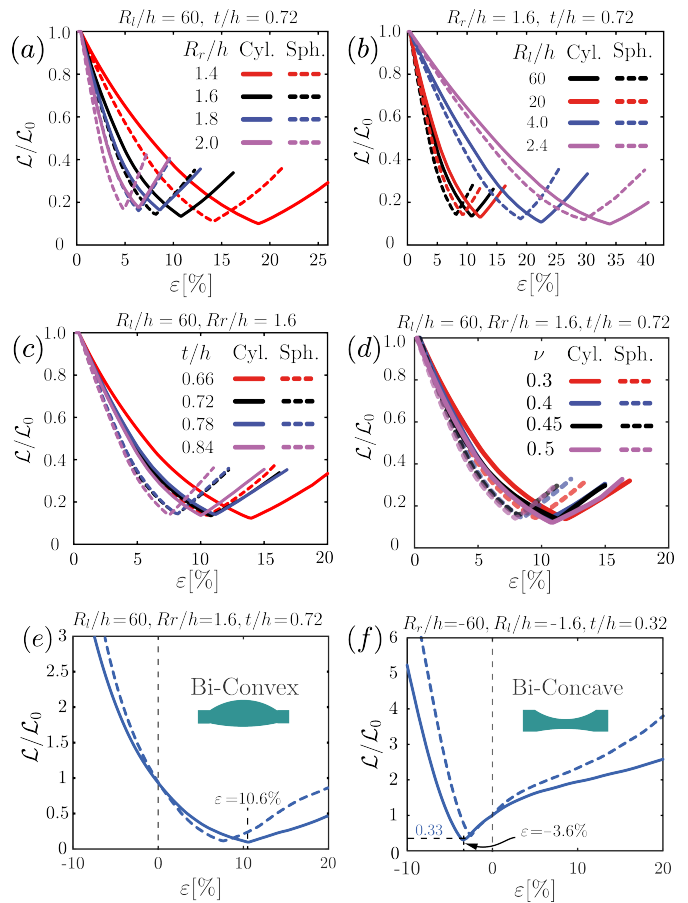


FIG. 4. Effect of geometry, material and loading direction on \mathcal{L} . (a)-(e) Effect of (a) R_r/h , (b) R_l/h , (c) t/h and (d) ν (note that $\nu = 0.5$ requires an incompressible strain energy function ψ - see Supporting Information for details) and (e) loading direction on \mathcal{L} for both cylindrical (solid lines) and spherical (dashed lines) bi-convex lenses. (f) Effect of loading direction on \mathcal{L} for a bi-concave lens.

To summarize, we have demonstrated that mechanical deformation can be harnessed to reduce spherical aberration of cylindrical/spherical bi-convex soft lenses. More specifically, we have used analyses to show that a critical strain exists for which the profile of the deformed lens closely approaches the shape of an aberration-free one and also demonstrated the concept experimentally. Although in this study we have focused on conventional biconvex/biconcave elastomeric lenses with initially smooth surfaces, **the proposed methodology is general and do not rely on any approximation, such as paraxial approximation or thin lens approximation. Therefore, it can be extended to design thin and thick unconventional lenses with irregular shapes as well as surface**

features (such as cuts, local bulges, or wrinkles) purposefully introduced to further alter the optical response. In parallel, it also enables investigation of different deformation protocols, such as twisting, shearing and extension followed by bending which has been showed to result in aberration reduction in thin lenses [28, 35, 36]. Further, generalizations can be achieved by exploring the effect of different materials. For example, by incorporating a temperature dependent visco-elastic model for glass [37–39], one could investigate the effect of deformation applied in the melted state on lenses made of glass, providing new routes for the realization of aberration-free lenses. Finally, while here we have considered spherical aberration,

the effect of deformation on different other optical properties, including tilt, coma and distortion, remains to be explored. Given these additional possibilities, we have made all our numerical codes available for download to be used and expanded upon by the community [40].

K.B. acknowledges support from the National Science Foundation under Grants No. DMR-2011754 and DMR-1922321. A.Z. thanks Iman Ranjbar for discussions on spherical aberration.

-
- [1] Emmanuel Siéfert, Etienne Reyssat, José Bico, and Benoît Roman. Bio-inspired pneumatic shape-morphing elastomers. *Nature materials*, 18(1):24–28, 2019.
- [2] Emmanuel Siéfert, Etienne Reyssat, José Bico, and Benoît Roman. Programming stiff inflatable shells from planar patterned fabrics. *Soft Matter*, 16(34):7898–7903, 2020.
- [3] Bastiaan Florijn, Corentin Coulais, and Martin van Hecke. Programmable mechanical metamaterials. *Physical review letters*, 113(17):175503, 2014.
- [4] Katia Bertoldi, Vincenzo Vitelli, Johan Christensen, and Martin Van Hecke. Flexible mechanical metamaterials. *Nature Reviews Materials*, 2(11):1–11, 2017.
- [5] Tianqi Xu, Jiachen Zhang, Mohammad Salehzadeh, Onaizah Onaizah, and Eric Diller. Millimeter-scale flexible robots with programmable three-dimensional magnetization and motions. *Science Robotics*, 4(29), 2019.
- [6] Aslan Miriyev, Kenneth Stack, and Hod Lipson. Soft material for soft actuators. *Nature communications*, 8(1):1–8, 2017.
- [7] Steven I Rich, Robert J Wood, and Carmel Majidi. Untethered soft robotics. *Nature Electronics*, 1(2):102–112, 2018.
- [8] Wenqi Hu, Guo Zhan Lum, Massimo Mastrangeli, and Metin Sitti. Small-scale soft-bodied robot with multimodal locomotion. *Nature*, 554(7690):81–85, 2018.
- [9] Beomjune Shin, Jonghyun Ha, Minhee Lee, Keunhwan Park, Gee Ho Park, Tae Hyun Choi, Kyu-Jin Cho, and Ho-Young Kim. Hygrobot: A self-locomotive ratcheted actuator powered by environmental humidity. *Science Robotics*, 3(14), 2018.
- [10] Stefano Palagi and Peer Fischer. Bioinspired micro-robots. *Nature Reviews Materials*, 3(6):113, 2018.
- [11] Stefano Palagi, Andrew G Mark, Shang Yik Reigh, Kai Melde, Tian Qiu, Hao Zeng, Camilla Parmegiani, Daniele Martella, Alberto Sanchez-Castillo, Nadia Kapernaum, et al. Structured light enables biomimetic swimming and versatile locomotion of photoresponsive soft microrobots. *Nature materials*, 15(6):647–653, 2016.
- [12] Todd Courtney, Michael S Sacks, John Stankus, Jianjun Guan, and William R Wagner. Design and analysis of tissue engineering scaffolds that mimic soft tissue mechanical anisotropy. *Biomaterials*, 27(19):3631–3638, 2006.
- [13] R Landers, A Pfister, U Hübner, H John, R Schmelzeisen, and R Mülhaupt. Fabrication of soft tissue engineering scaffolds by means of rapid prototyping techniques. *Journal of materials science*, 37(15):3107–3116, 2002.
- [14] Douglas P Holmes and Alfred J Crosby. Snapping surfaces. *Advanced Materials*, 19(21):3589–3593, 2007.
- [15] GC Knollman, JLS Bellin, and JL Weaver. Variable-focus liquid-filled hydroacoustic lens. *The Journal of the Acoustical Society of America*, 49(1B):253–261, 1971.
- [16] Hongwen Ren and Shin-Tson Wu. Variable-focus liquid lens. *Optics Express*, 15(10):5931–5936, 2007.
- [17] Luca Wallace V De. Variable power fluid lens, December 15 1964. US Patent 3,161,718.
- [18] Samuel Shian, Roger M Diebold, and David R Clarke. Tunable lenses using transparent dielectric elastomer actuators. *Optics express*, 21(7):8669–8676, 2013.
- [19] Federico Carpi, Gabriele Frediani, Simona Turco, and Danilo De Rossi. Bioinspired tunable lens with muscle-like electroactive elastomers. *Advanced Functional Materials*, 21(21):4152–4158, 2011.
- [20] Kazunori Hoshino and Isao Shimoyama. Analysis of elastic micro optical components under large deformation. *Journal of Micromechanics and Microengineering*, 13(1):149, 2002.
- [21] Stefan Schuhladen, Sebastian Petsch, Peter Liebetraut, Philipp Müller, and Hans Zappe. Miniaturized tunable imaging system inspired by the human eye. *Optics letters*, 38(20):3991–3994, 2013.
- [22] Jong-Moon Choi, Hyung-Min Son, and Yun-Jung Lee. Biomimetic variable-focus lens system controlled by winding-type sma actuator. *Optics express*, 17(10):8152–8164, 2009.
- [23] Peter Liebetraut, Sebastian Petsch, Wolfgang Mönch, and Hans Zappe. Tunable solid-body elastomer lenses with electromagnetic actuation. *Applied optics*, 50(19):3268–3274, 2011.
- [24] Luc Maffli, Samuel Rosset, Michele Ghilardi, Federico Carpi, and Herbert Shea. Ultrafast all-polymer electrically tunable silicone lenses. *Advanced functional materials*, 25(11):1656–1665, 2015.
- [25] Alan She, Shuyan Zhang, Samuel Shian, David R Clarke, and Federico Capasso. Adaptive metalenses with simultaneous electrical control of focal length, astigmatism, and shift. *Science advances*, 4(2):eaap9957, 2018.
- [26] Michele Ghilardi, Hugh Boys, Peter Török, James JC Busfield, and Federico Carpi. Smart lenses with electrically tunable focal length. *Optics express*, 17(10):8152–8164, 2009.

- cally tuneable astigmatism. *Scientific reports*, 9(1):1–10, 2019.
- [27] Peter Liebetraut, Sebastian Petsch, Jens Liebeskind, and Hans Zappe. Elastomeric lenses with tunable astigmatism. *Light: Science & Applications*, 2(9):e98, 2013.
- [28] Gérard René Lemaître. *Astronomical optics and elasticity theory: active optics methods*. Springer Science & Business Media, 2008.
- [29] Florian Rathgeber, David A. Ham, Lawrence Mitchell, Michael Lange, Fabio Luporini, Andrew T. T. McRae, Gheorghe-Teodor Bercea, Graham R. Markall, and Paul H. J. Kelly. Firedrake: automating the finite element method by composing abstractions. *ACM Trans. Math. Softw.*, 43(3):24:1–24:27, 2016.
- [30] Rudolf Karl Luneburg. *Mathematical theory of optics*. Univ of California Press, 1966.
- [31] Ernest George Coker and Louis Napoleon George Filon. *A Treatise on Photo-elasticity*. University Press, 1931.
- [32] Note that the aberration measure \mathcal{L} used here is closely related to the wavefront aberration measurement defined by the Zernike polynomials (i.e., spherical polynomial coefficient or Z_4^0) [33].
- [33] Max Born and Emil Wolf. *Principles of optics: electromagnetic theory of propagation, interference and diffraction of light*. Elsevier, 2013.
- [34] Since the surface profile of a lens with zero aberration obtained by equating Eq. (2) and (4) is not unique [41], we fix one of the two profiles.
- [35] Gerard R Lemaître. Optical design and active optics methods in astronomy. *Optical Review*, 20(2):103–117, 2013.
- [36] Pengpeng Zhao, Çağlar Ataman, and Hans Zappe. Spherical aberration free liquid-filled tunable lens with variable thickness membrane. *Optics Express*, 23(16):21264–21278, 2015.
- [37] Masahiro Arai, Yuusuke Kato, and Tsutomu Kodera. Characterization of the thermo-viscoelastic property of glass and numerical simulation of the press molding of glass lens. *Journal of Thermal Stresses*, 32(12):1235–1255, 2009.
- [38] Anurag Jain and Allen Y Yi. Numerical modeling of viscoelastic stress relaxation during glass lens forming process. *Journal of the American Ceramic Society*, 88(3):530–535, 2005.
- [39] Allen Y Yi and Anurag Jain. Compression molding of aspherical glass lenses—a combined experimental and numerical analysis. *Journal of the American Ceramic Society*, 88(3):579–586, 2005.
- [40] Hyperelastic lens aberration (hela). <https://github.com/ahmadzareei/HELA>, 2020.
- [41] Rafael G González-Acuña and Julio C Gutiérrez-Vega. General formula for aspheric collimator lens design free of spherical aberration. In *Current Developments in Lens Design and Optical Engineering XX*, volume 11104, page 111040P. International Society for Optics and Photonics, 2019.